Electronic Supplementary Material (ESI) for Chemical Communications

CeO_2 Nanoplates with a Hexagonal Structure and Their Catalytic Applications in Highly Selective Hydrogenation of Substituted Nitroaromatics

Yu Zhang, Fei Hou, and Yiwei Tan*

State Key Laboratory of Materials-Oriented Chemical Engineering, School of Chemistry and Chemical Engineering, Nanjing University of Technology, Nanjing 210009, China, e-mail: ytan@njut.edu.cn

Experimental Section

Materials. All chemicals were commercially available reagents and used as received. Cerium(III) acetate sesquihydrate (99.9%), *p*-anisidine (99%), *o*-anisidine (99%), 1,3-dinitrobenzene (99%), 4-nitrobenzoic acid (99%), 3-nitrostyrene (96%), 4-nitroacetophenone (98%), and 4-nitro-1H-pyrazole-3-carboxylic acid (98%) were purchased from Alfa Aesar. Palladium(II) acetylacetonate ($Pd(acac)_2$, 99%), copper(II) acetylacetonate ($Cu(acac)_2$, 99%), and oleylamine (70%) were purchased from Sigma-Aldrich.

Synthesis of CeO_2 Nanoplates. *Hexagonal Nanoplates*. Typically, 20 mL of an aqueous solution of cerium(III) acetate sesquihydrate (8.0 mM) was added into 20 mL of an aqueous solution of *o*-anisidine or *p*-anisidine (12.0 mM) in a 45 mL Teflon-lined autoclave under vigorous stirring. Afterward, the autoclave was sealed and maintained at 250 °C for 6 h and subsequently cooled to ambient temperature naturally. The as-prepared CeO_2 nanoplates settled at the bottom of the autoclave were fully dispersed in 5 mL of *N*-methyl-2-pyrrolidone at 50 °C for 8 h. This process was repeated for 5–6 times to remove the adsorbed poly(*o*-anisidine) or poly(*p*-anisidine). Finally, the products were washed with ethanol many times and dried. The same ceria nanoplates were obtained within a cerium(III) acetate concentration window of 8.0–16.0 mM.

Triangular Nanoplates. The experimental procedure was the same as that described above for the preparation of hexagonal nanoplates except the presence of $Pd(acac)_2$ (45 μmol/L) in the initial reaction mixture.

Synthesis of CuPd/CeO_2 Nanoplates. *CuPd Nanoalloys*. $Pd(acac)_2$ (0.075 mmol), $Cu(acac)_2$ (0.075 mmol), and aniline (1.80 mmol) were mixed together with oleylamine (15.0 mL) in a 50 mL three-neck round-bottom flask equipped with a condenser and attached to a Schlenk line and purged of air by three cycles of evacuation and followed by blowing a nitrogen stream. The mixture turned into a transparent grey green color after the flask was heated to 120 °C. Subsequently, the solution was heated to 220 °C at a heating rate of ~20 °C/min and maintained at this temperature for 15 min with vigorous magnetic stirring under a nitrogen atmosphere. Finally, the black solution was cooled down to room temperature naturally by removing the reaction flask from the heating mantle. The CuPd alloy nanoparticles were isolated by precipitating the colloids from the final reaction solution using 30 mL of ethanol. The precipitates were washed with 10 mL of ethanol again. Finally, the precipitates were redissolved in 25.0 mL of hexane. The CuPd nanoparticle composition and content were determined to be Cu:Pd = 56:44 and 0.024 M by ICP-AES measurement.

CuPd/CeO_2 Nanoplate Catalyst. 10.0 mL of CuPd nanoalloy solution in hexane aforementioned was blended with 100.0 mg CeO_2 nanoplate powder by sonication for 10 min at room temperature. After evaporation of the solvent, a gray paste was obtained. This paste was washed with cyclohexane to remove the free metal for three times and dried under vacuum at room temperature. CuPd loading of the ceria nanoplate-supported catalyst (CuPd/CeNP) was 15wt % through ICP-AES measurement.

Characterization. Shape and size of the products were analyzed using a Hitachi S-4800 field-emission scanning electron microscope (SEM) operated at 5 kV. Transmission electron microscopy (TEM) micrographs, particulate size distribution, lattice structure, and energy-dispersive X-ray

spectroscopy (EDX) were obtained by using a JEOL 1010 and a FEI Tecnai G2 F20 S-Twin transmission electron microscope, operated at 80 and 200 kV, respectively. The specimens for TEM were prepared by dispersing the products in 2-propanol, and then drop-casting the dispersions onto ultrathin carbon-coated copper grids. Powder X-ray diffraction (XRD) patterns were recorded on a Rigaku D/max-2400 diffractometer operated at 40 kV voltage and 200 mA current with Cu Kα radiation (λ = 1.5406 Å). X-ray photoelectron spectrometer (XPS) measurements were carried out in an ion-pumped chamber (evacuated to 6.7×10^{-8} Pa) of an PHI5000 VersaProbe (Japan, ULVAC–PHI) spectrometer, employing a monochromatized microfocused Al-Kα X-ray source. The binding energy (BE) for the samples was calibrated by setting the measured BE of C 1s to 284.6 eV.

Catalysis Studies. The catalytic hydrogenation reactions were done in batch mode and carried out in a 100 mL batch reactor equipped with a glandless magnetically driven, six-bladed turbine agitator, a thermocouple, two baffles, a cooling coil, a gas inlet, and external electrical heating arrangement. Typically, the reaction mixture and the 15 wt % CuPd/CeNP catalyst (catalyst loading: 3 wt % of the substrate) are introduced into the batch reactor. Subsequently, the reactor was purged with H_2 for three times at room temperature to remove air from the reactor, and then hydrogenation reactions were carried out with magnetic stirring (600 rpm) under 1 bar of H_2 after the reactor was heated to a required temperature (see Table 1). Once the reaction was completed, the reactor was cooled down and its content was transferred into a vial. For each substrate, the same catalysis testing procedure was followed for each run. Supernatants obtained by centrifugation of the sampled mixtures were analyzed using HPLC to determine the amount of product and the remaining substrate. To monitor the conversion of the substrate, aliquots of the reaction mixture was withdrawn, filtered, and analyzed by liquid chromatography (Hewlett-Packard 1100 using a ZORBAX Eclipse XDB-C18 column) and gas chromatography-mass spectrometry (GC-MS, TRACE DSQ).

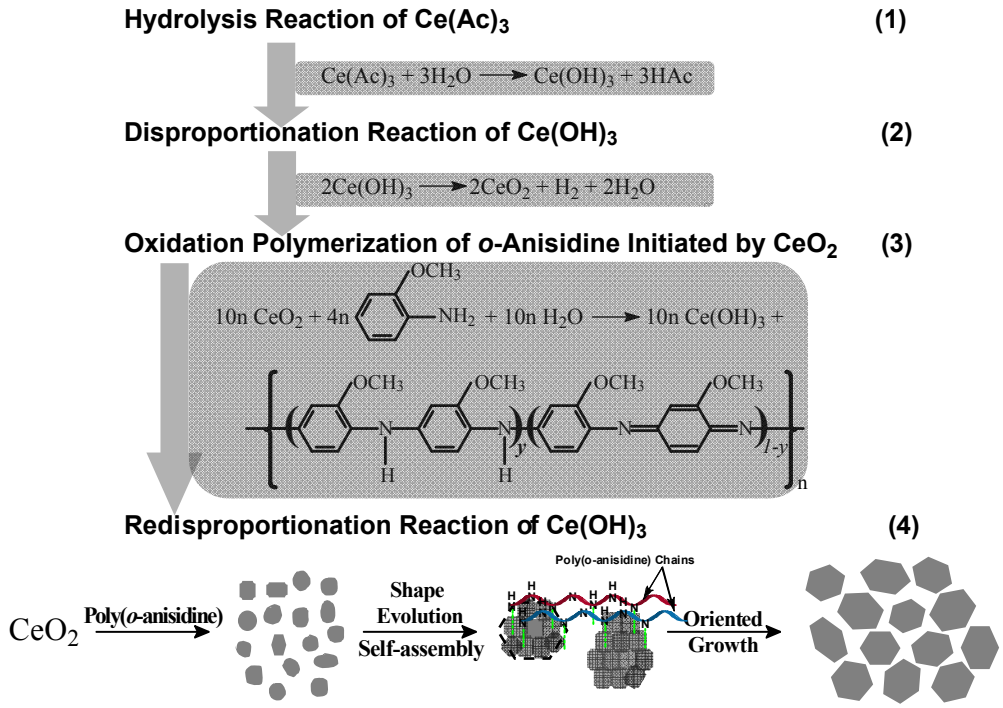

Figure S1. Schematic representation of the process involved in the formation of CeO_2 nanoplates under the hydrothermal conditions.

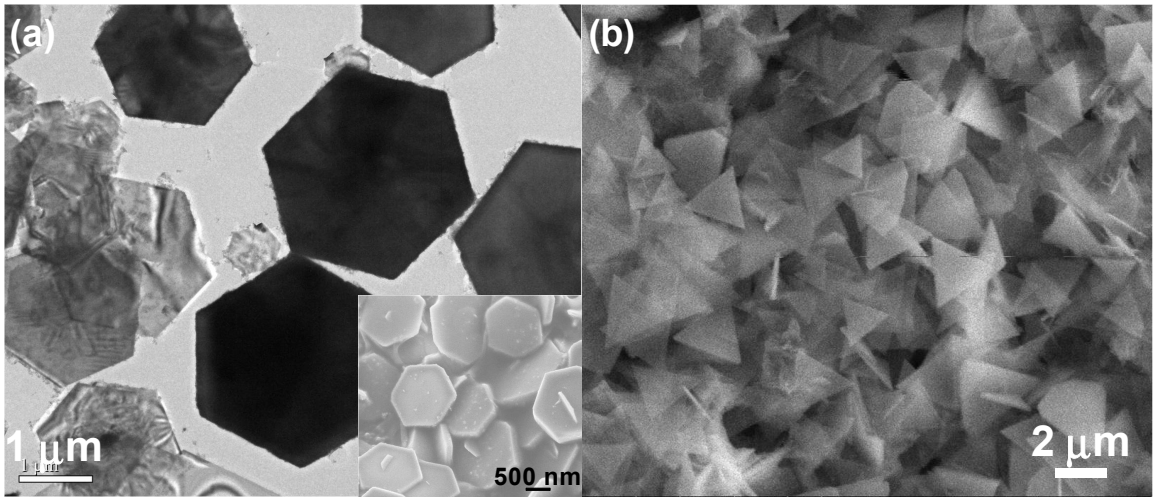

Figure S2. (a) TEM image and (b) SEM image of the CeO_2 nanoplates with hexagonal and triangular shape. The inset in panel a shows a magnified SEM image of the CeO_2 nanoplates.

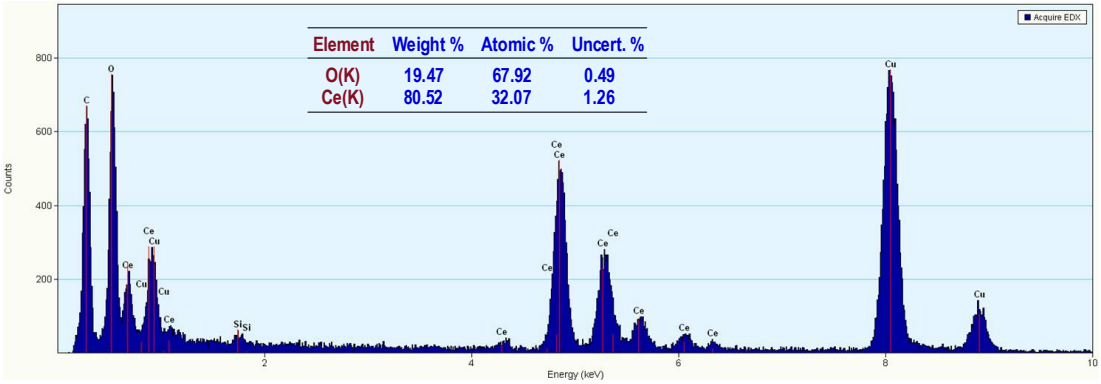

Figure S3. EDX spectrum recorded from the hexagonal CeO_2 nanoplates.

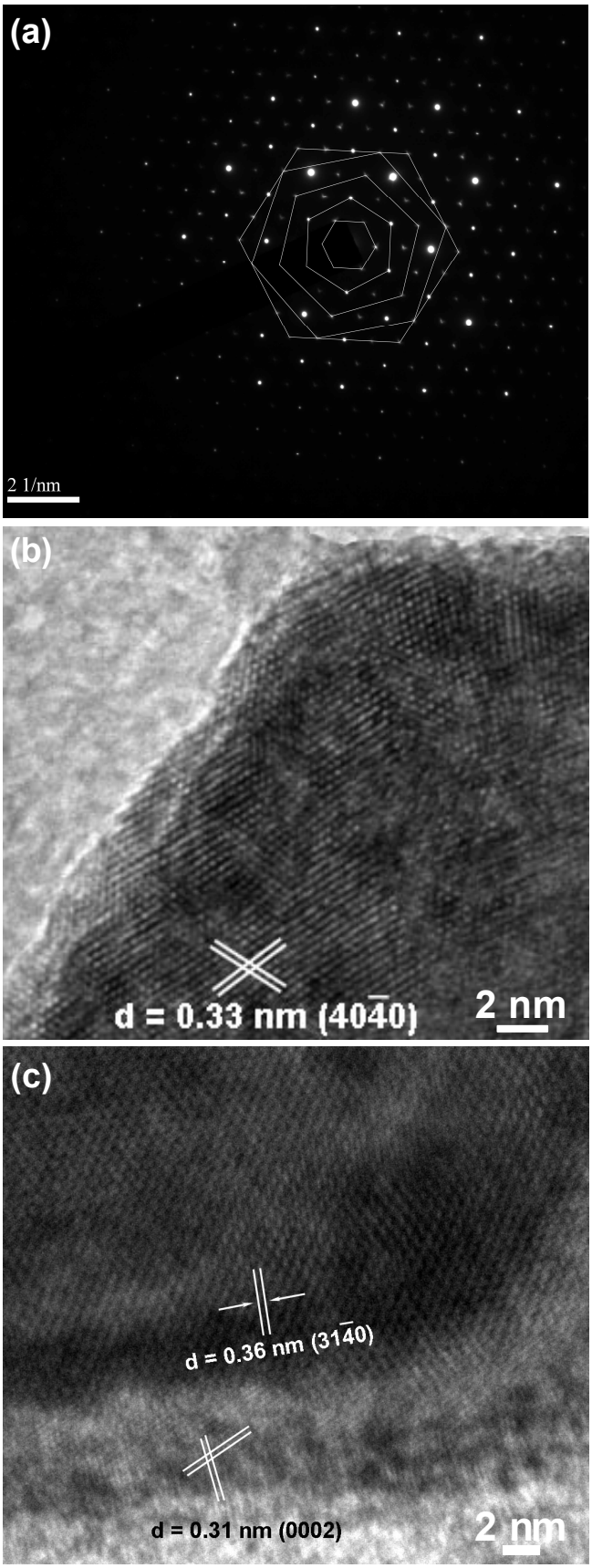

Figure S4. (a) SAED pattern recorded from the hexagonal CeO_2 nanoplates, (b) [0001] HRTEM image at the edge region of a nanoplate, and (c) HRTEM image of a CeO_2 nanoplate tilted 10° from the incident electron beam. The edge regions of the nanoplates in the HRTEM images reveal that the nanoplates consist of multiple layers stacked along the *c*-axis.

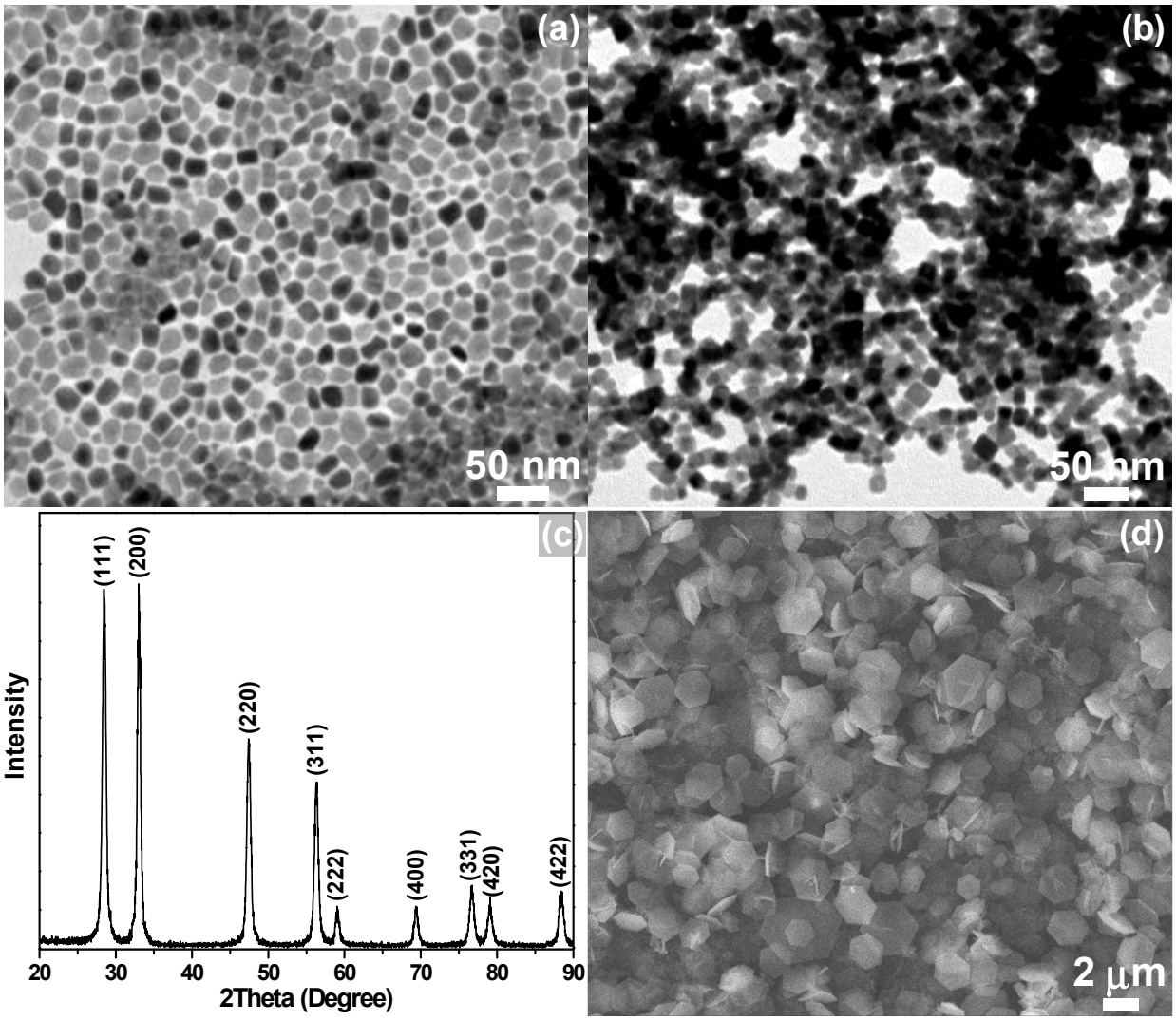

Figure S5. TEM images of the CeO_2 nanoparticles collected after a different reaction period of (a) 2 h and (b) 4 h. (c) The corresponding XRD pattern of the CeO_2 nanoparticles shown in panel b, in which the enhanced (200) peak intensities came from the (100) facets as a result of the preferred orientation of the cubic CeO_2 nanocrystals. SEM images of the CeO_2 nanoplates with (d) hexagonal shape synthesized after a reaction time of 6 h.

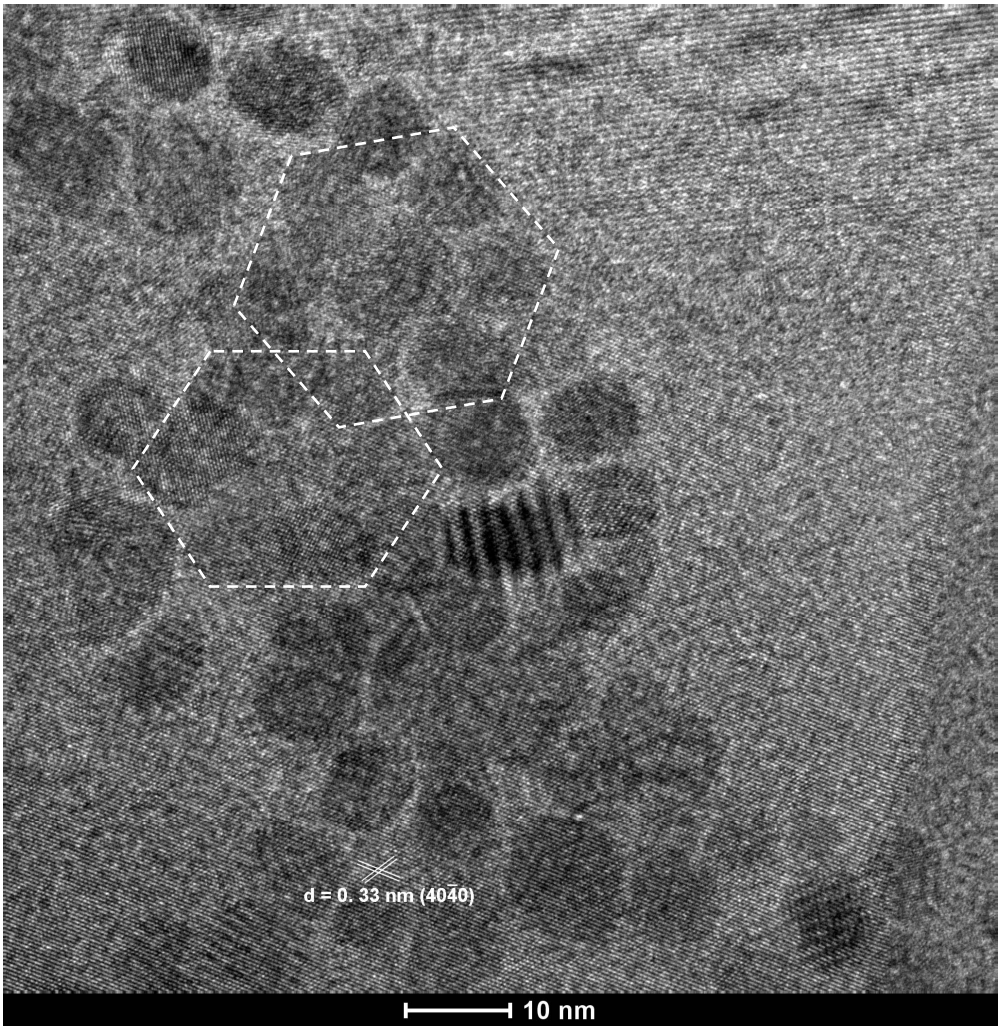

Figure S6. HETEM image presents the oriented attachment of CeO_2 nanocubes on the surface of a CeO_2 nanoplate. The indicated regions imply the formation process of the CeO_2 nanoplates with a hexagonal shape.

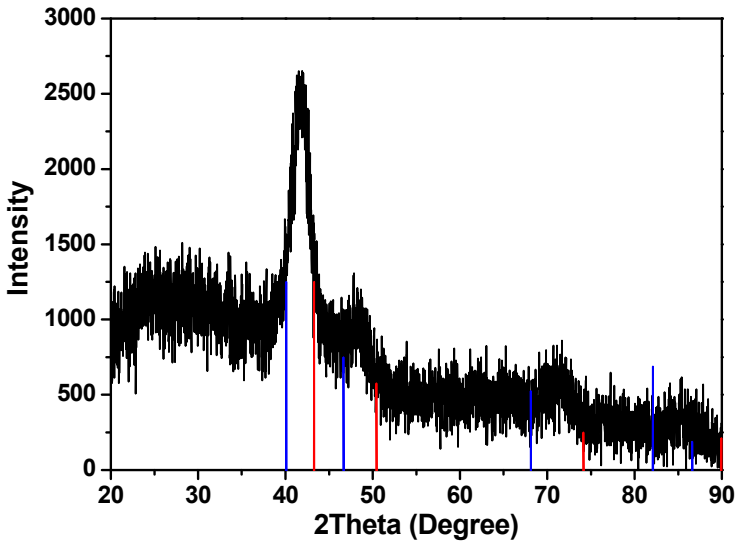

Figure S7. XRD patterns of the CuPd nanoparticles with peak positions that are intermediate between those of Cu and Pd, which suggests an approximate composition of $Cu_{54}Pd_{46}$ on the basis of Vegard's law. The average crystal domain size of 5.2 nm, determined by the peak widths in the XRD pattern based on the Scherrer equation, is consistent with the average particle size analyzed by TEM measurements (see below).

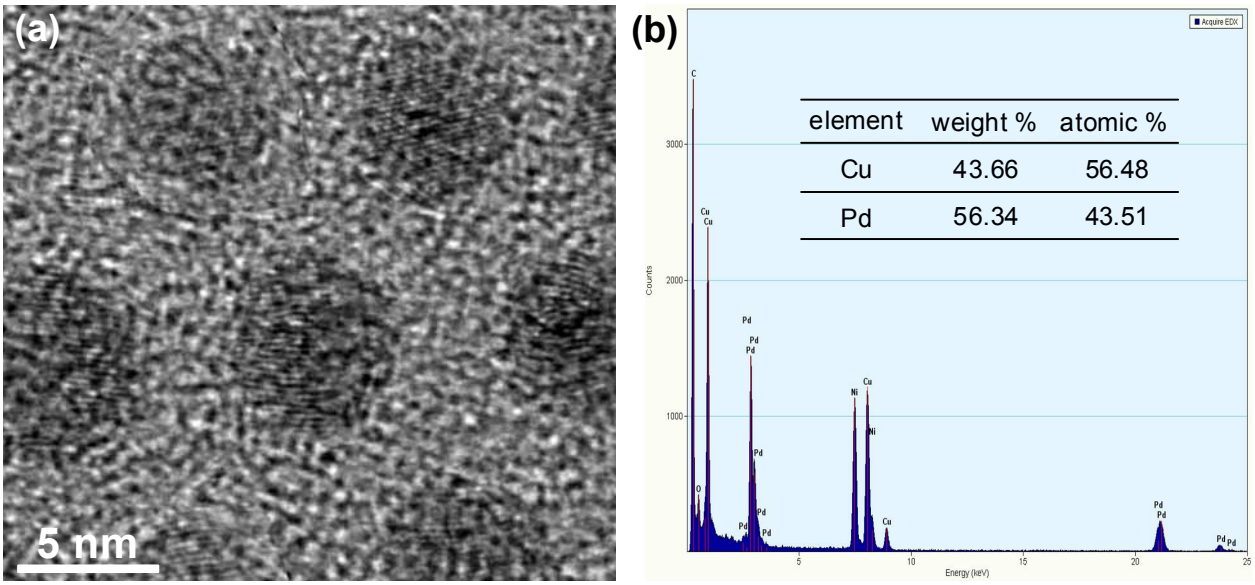

Figure S8. (a) HRTEM image of CuPd nanoparticles reveals the single-crystalline nature of most the as-prepared nanoparticles, which is evidenced by the continuous lattice spacing of 2.19 Å corresponding to those {111} planes of fcc CuPd. (b) EDX spectrum of the CuPd nanocrystals. The specimens for HRTEM characterization were prepared by placing one drop of nanoparticle solution in hexane onto 300-mesh carbon-coated nickel grids.

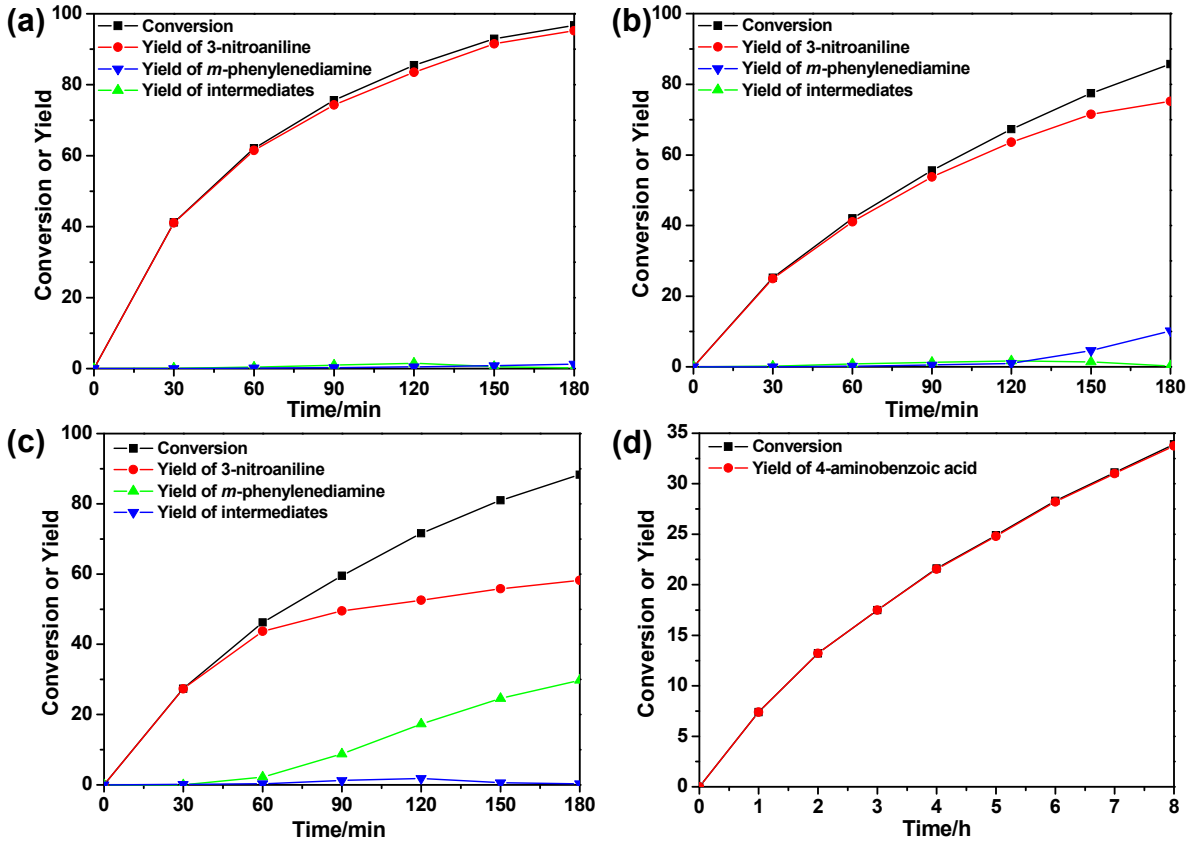

Figure S10. Evolution of the catalytic hydrogenation of (a–c) 1,3-dinitrobenzene and (d) 4-nitrobenzoic acid versus time in acetone solvent using (a) CuPd/CeNP, (b) CuPd/TiO_2(P25), and (c,d) CuPd/CeO_2 nanocubes (fluorite structure) as the catalyst. Reaction conditions: substrate, 0.065 mol/L; catalyst, 15 wt % CuPd/CeNP; catalyst loading, 3 wt % of the substrate; temperature, 40 °C for 1,3-dinitrobenzene and 60 °C for 4-nitrobenzoic acid; P_{H2}, atmospheric pressure; solvent, acetone; reaction volume, 50 mL.

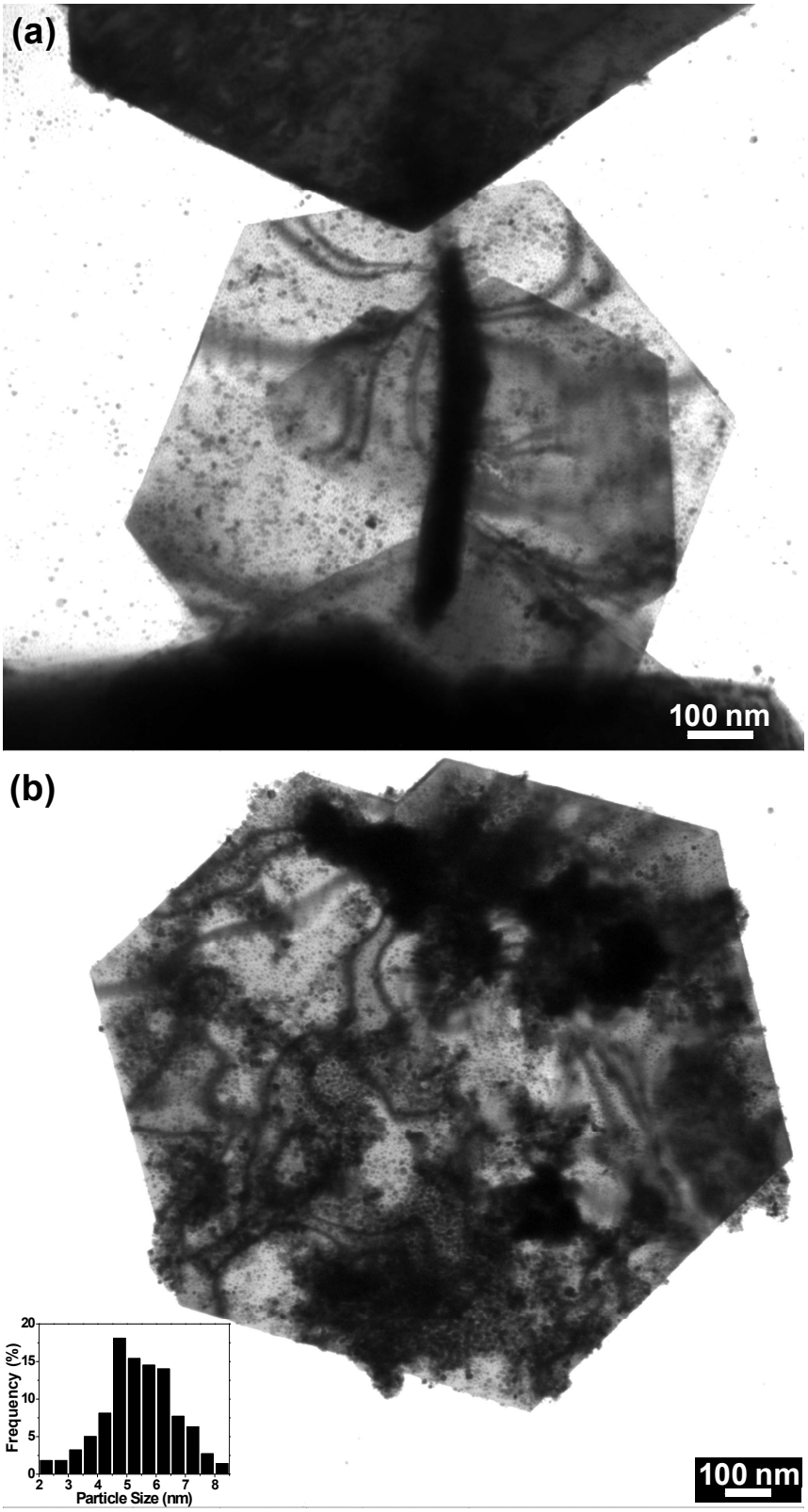

Figure S9. (a,b) TEM images of the CuPd nanoparticles supported on the CeO_2 nanoplates. The inset in panel b exhibits the CuPd particle size distribution. Accordingly, the average particle size is calculated to be 5.3 nm. The large, high contrast features on the nanoplates are the overlapped nanoparticles.

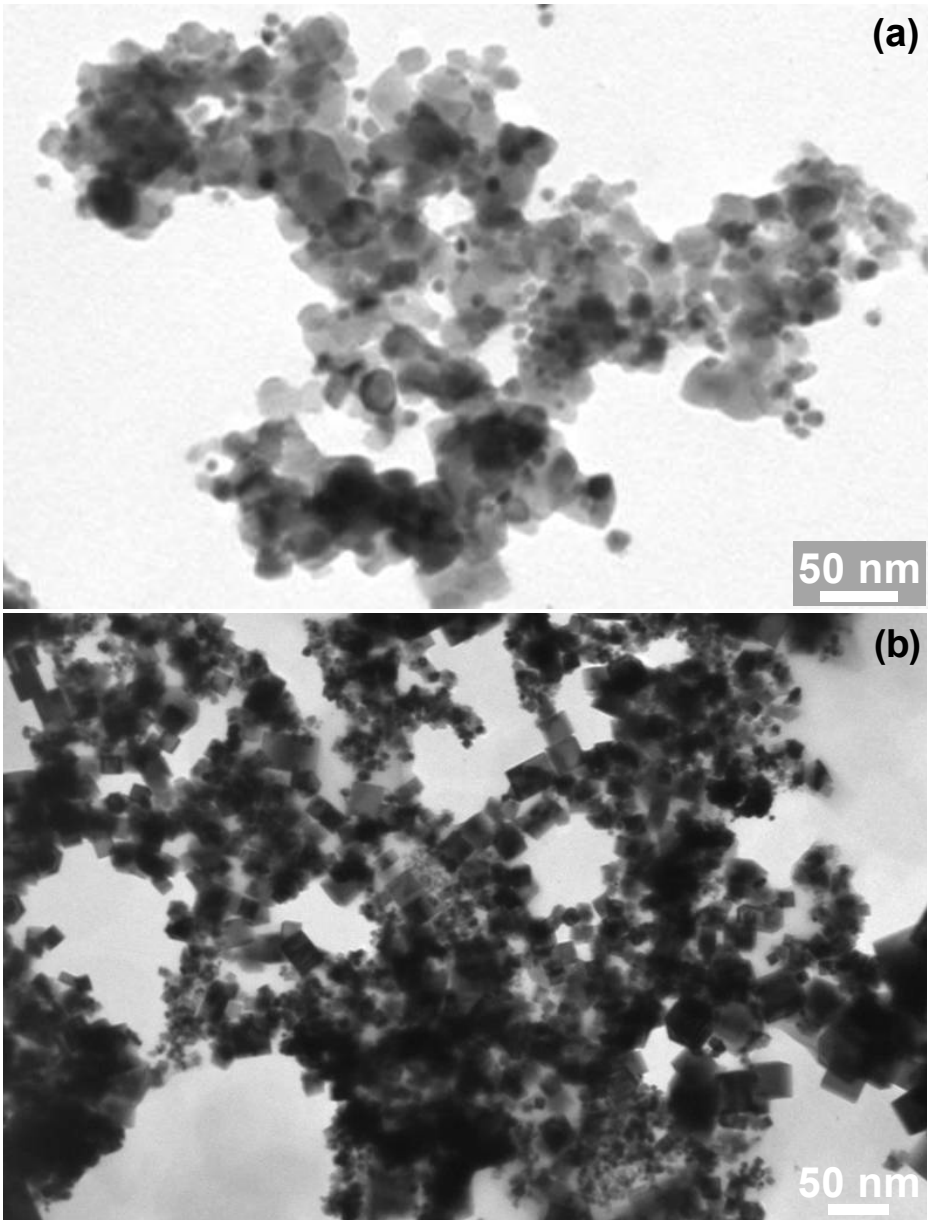

Figure S11. TEM image of CuPd nanoparticles supported on (a) TiO_2 and (b) CeO_2 nanocubes.

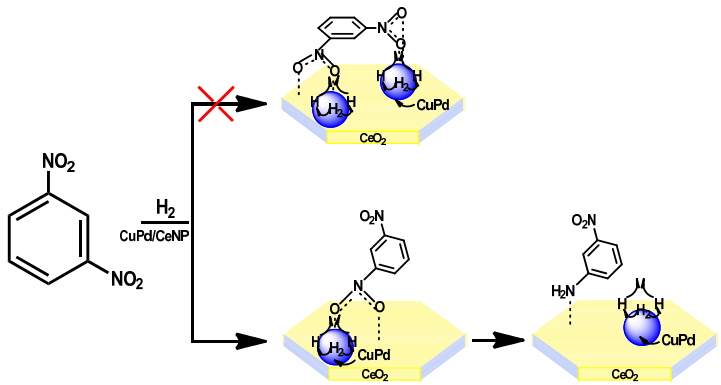

Figure S12. Possible Reaction Mechanism for the Selective Hydrogenation of 1,3-Dinitrobenzene over the CuPd/CeNP Catalyst.

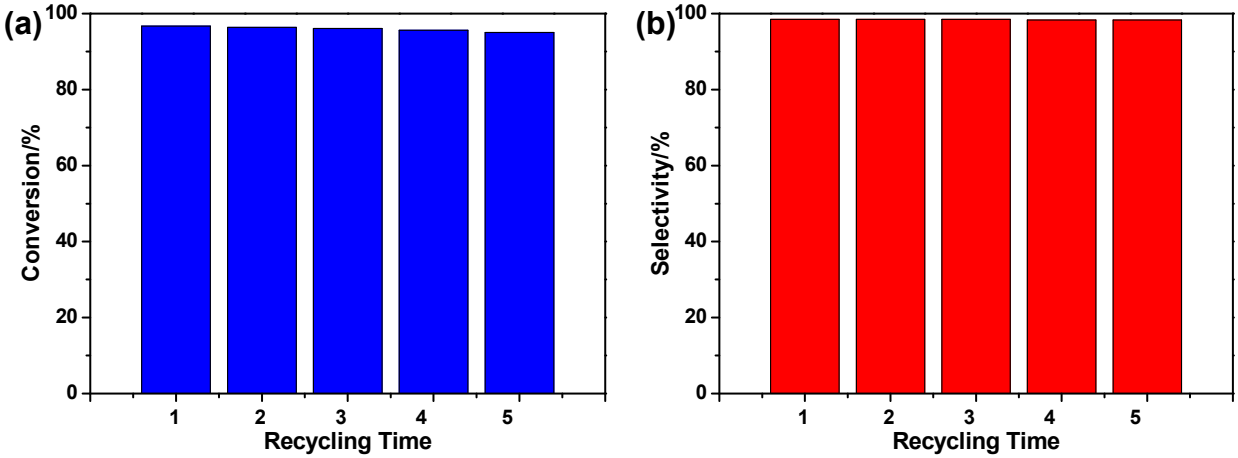

Figure S13. Effects of recycling the CuPd/CeNP catalyst on the conversion and selectivity of 1,3-dinitrobenzene.

Table S1. Catalytic Activities for Hydrogenation of Substituted Nitroaromatics Using CuPd@CeNP Catalyst under Different Conditions [a]

entry	Substrate	temperature (°C)	time (h)	conv. (%)	product	sel. (%)
1		40	3.5	96.7		98.5
2	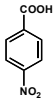	60	8.5	99.5	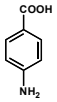	>99
3		40	8.5	99.0		>99
4	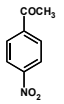	55	5.6	99.5	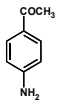	>99
5		55	5.0	99.0		99

[a] Reaction conditions: substrate, 0.065 mol/L; catalyst, 15 wt % CuPd/CeNP; catalyst loading, 3 wt % of the substrate; P_{H2}, atmospheric pressure; solvent, acetone; reaction volume, 50 mL.

Table S2. Effects of various experimental parameters on the conversion and selectivity of 1,3-dinitrobenzene

Entry	solvent (50 mL)	temperature (°C)	time (h)	conv. (%)	sel. (%)	
					3-nitroaniline	*m*-phenylenediamine
1	ethanol	25	4.3	35.9	95.4	4.6
2	ethanol	40	3.5	75.2	93.1	6.9
3	ethanol	50	3.0	95.8	86.4	13.6
4	ethanol	60	3.5	99.9	81.6	18.4
5	methanol/H_2O (3:7 v/v)	95	5.0	7.9	59.7	41.3
6	methanol/H_2O (3:7 v/v)	95	2.0	0	N/A	N/A

Reaction conditions: substrate, 0.065 mol/L; catalyst, 15 wt % CuPd/CeNP; catalyst loading, 3 wt % of the substrate; P_{H2}, atmospheric pressure.

Table S3. Effects of various experimental parameters on the conversion and selectivity of 4-nitrobenzoic acid into 4-aminobenzoic acid

entry	solvent	temperature (°C)	time (h)	conv. (%)	sel. (%)
1	ethanol	40	8.0	61.5	99.1
2	ethanol	65	8.0	78.7	99.2
3	methanol/H_2O (3:7 v/v)	90	8.5	0	N/A

Reaction conditions: substrate, 0.065 mol/L; catalyst, 15 wt % CuPd/CeNP; catalyst loading, 3 wt % of the substrate; P_{H2}, atmospheric pressure.